Geometrical measurement of real foams from 3D images

Emmanuel Brun , Jérôme Vicente, Frédéric Topin, René Occelli
IUSTI Laboratory- CNRS UMR 6595 – Polytech Marseille
5, rue enrico Fermi, 13453 Marseille cedex 13 France

ABSTRACT

This paper presents the specific morphological methods developed to measure geometrical characteristic of metallic foams. Several parameters (porosity, specific surface, pore diameter…) that are commonly used to describe the texture of such media are not sufficient. Structural properties (throat diameter, strut lengths, tortuosity,…) are also necessary to complete these descriptions as local topology may have a strong influence on properties (e.g. permeability, radiative properties..). Two independent network associated to each phase are constructed from the actual structure. The pore network is simply obtained by joining adjacent individualized cells. These cells are segmented using watershed method on the distance map. Markers are obtained starting from maximal included sphere determination.

INTRODUCTION

Due to their novelty, their complex three-dimensional structure and varied manufacturing processes, metal foams properties are still incompletely characterized. Thermo-physical and flow properties strongly depend on local morphology of both pores and solid matrix. Local changes (e.g. constriction, strut cross section, surface roughness…) of the structure can influence properties. Most of the modeling approaches are based on arbitrary periodic structures, which represent the texture of the foam. There is a lack of morphological tools to characterize the real microstructures of these foams and very few works use the real geometry (usually obtained from 3D X-ray tomography) to determine physical properties [1-3].
We present results on a representative set of commercially available foam. All method and results will be fully discussed and compared to available literature data.

SAMPLES

We work on a set of Recemat Nickel-Chromium (NC) and reinforced Nickel-Chromium (NCX) foam samples. We used cylindrical samples (40mm and 16mm diameter, and thickness 13mm and 6mm (Table 1)). Sample size was maximized in respect with data volume constraint and X-ray images resolution in order to have a large number of cells and detect efficiently hollow struts. High-resolution microtomographic acquisition was performed on the ID19 beam line of the European Synchrotron Radiation Facility (ESRF, Grenoble, France). The FRELON CCD camera, developed at ESRF, allows 2048 x 2048 pixels radiographs. An initial set-up was selected to provide a pixel size of 29.47 µm2 in order to acquire the totality of our 40mm diameter samples and a size of 7.46µm for our 16 mm diameter samples.

GEOMETRICAL CHARACTERIZATION OF THE FLUID PHASE

To access the structural properties of the foam we need to segment our images. The pore segmentation consists in individualizing each cell. The method is based on the 3D watershed transform [4] on the pore distance map. The quality of the cell segmentation depends on the automatic markers extraction. [5] used topographic conditions based on markers neighborhood analysis, but several parameters have to be adjusted depending on the analyzed foam. We improve this method using an automatic marker extraction based on the maximal included ball [6]. We construct an augmented aperture map (both diameter and label of the maximal ball are assigned to each voxel). As cells present roughly ellipsoid shape, we suppose that each one contains only one totally included maximal ball. We then keep only one marker by balls, and eliminate redundant markers associated to incomplete balls. Watershed transform is then applied on the pore distance map using the markers extracted as mentioned above.

Segmentation of pores in individualized cells gives access to detailed morphometry and orientations measurement. The volume of each cell is simply obtained by counting the voxels of our segmented image. Figure 1 shows the pore diameter (diameter of the sphere of equivalent volume) distribution on the 4 different foams.
The Gaussian law distribution permits to define a mean diameter for each sample (cf table 2).

Table I : Samples description

Samples	Original X-ray images					Reduced images for analysis			
	Sample diameter	voxel size	image size	images number	thickness	voxel size	image size	images number	Cells number
(material-ppi)	(mm)	(µm)	pixels		(mm)	(µm)	pixels		
NC-1116	40	29.47	1326	291	8.57	58.94	663	145	1638
NCX-1723	40	29.47	1326	348	10.25	58.94	663	140	3240
NCX-2733	16	7.46	2048	430	3.2	29.84	512	107	1832
NCX-3743	16	7.46	2048	292	2.18	29.84	512	73	3989

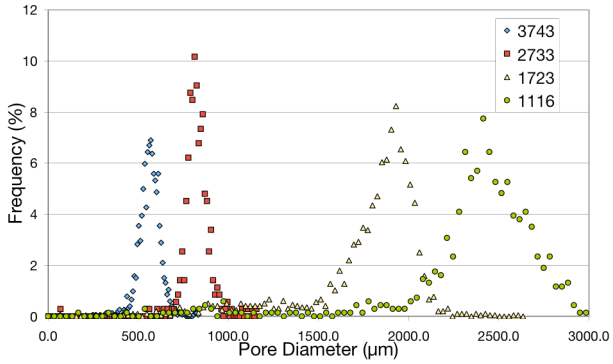

Figure 1. Pore diameter distribution

Throat diameter is a pertinent parameter to understand fluid flow properties of the media [7]. Throat surface is deduced from our segmentation by counting voxels belonging to two adjacent cells.

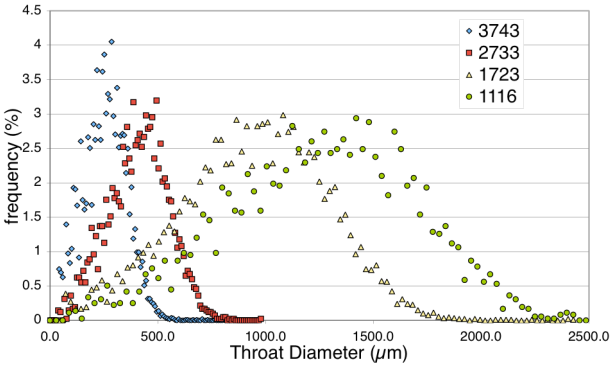

Figure 2. Throats Diameter distribution

Figure 2 shows the throat diameter (diameter of the disk of equivalent surface) distribution on all foams. The throat distribution is more scattered than the pore one.
From the segmented image we construct a vertex-edge graph to compute thermal effective conductivity on idealized network [7] but also to characterize the phase structurally. The nodes of this graph are cell centers and throats barycenters. We create edges by joining adjacent individualized cells and their surroundings throats. This data structure allows to measure geometrical properties (such as cells distance) and structural properties (e.g. network connectivity, tortuosity…).

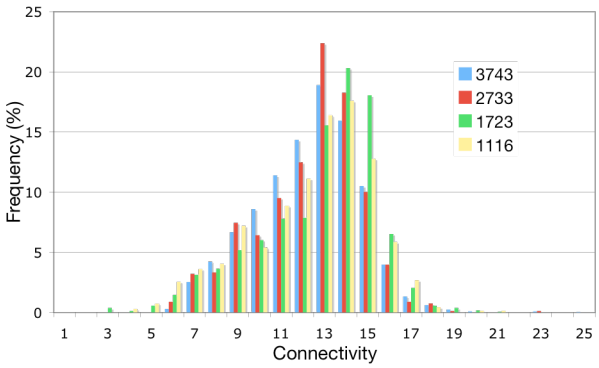

Figure 3. Connectivity of fluid Network

The figure 6 is a histogram of the connectivity of our fluid network. In other words it presents the number of cells a pore is connected to. Watching the graph we might say that representing foams by regular dodecahedron gives an incomplete idea of the structure.

SOLID PHASE CHARACTERIZATION

The solid phase characterization is based on its skeleton. We previously used the Distance Ordered Homotopic Thinning to obtain the 3d skeleton and thus the graph of the solid structure [8]. The main difficulty with thin line skeletization technique may be the over-segmentation that often occurs at struts intersections. The cleaning process necessary to eliminate false ligament is also non-trivial. Moreover, this method needed filled struts to give good results. Consequently we choose a new methodology, which associates each solid strut with its surrounding cells to obtain the solid matrix skeleton.

The solid phase skeleton is obtained from the previous cell segmentation. To identify nodes and ligaments, cells are inflated using an augmented fast Marching method [9]. Cells labels are propagated until all voxels are assigned. To retrieve the solid structure, voxels of these images are selected according to the Plateau's law. Plateau indicated that edges are formed by three liquid films equally inclined toward one another, and that vertices are formed by four edges equally inclined. Thus, voxels in our resulting inflated images, which have 3 different cell's label, in their 27 neighbor voxels, are edges. Nodes are voxels with 4 different labels. Throats are easily identified by voxels

with only 2 different labels. Only nodes are kept to reconstruct the entire solid graph. Labels of adjacent cells are assigned to each node. The solid ligaments are thus obtained by connecting nodes, which have in common at least 3 of their 4 labels. Metallic foam is thus described using a vertex-edge.

Solid ligament are modelized by the network edge, their length are reported on figure 4 and table 2.

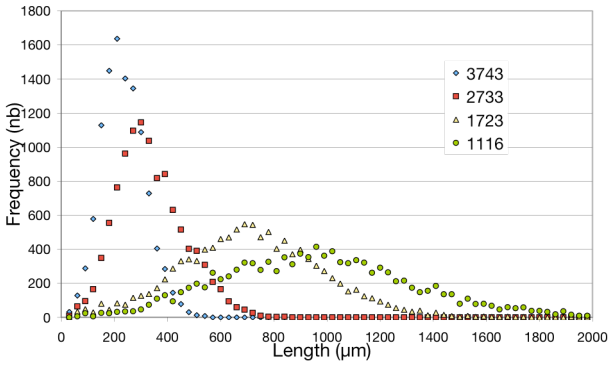

Figure 4. Strut length histogram

As expected to the Plateau's law we obtain for each sample a skeleton's connectivity equal to 4.

The tables 2 presents mean values of pore and throat diameter for each foam.

Table II : Geometrical measurement

Samples	1116	1723	2733	3743
Number of cells	684	1954	354	1522
Mean Pore Diameter (µm)	2356	1763	822	559
Standard Deviation	409	315	67	58
Number of Throats	3574	8710	4164	10171
Mean throat Diameter (µm)	1244	932	405	252
Standard Deviation	434	337	137	97
Number of struts	10768	28000	13390	34368
Mean strut length (µm)	950	725	318	222
Standard Deviation	360	269	124	81

Geometrical measurements presented in this part are at the cell scale, we present in the following structural measurement at the sample scale.

CELLS ORGANISATION AND ANISOTROPY MEASUREMENT

Cells structure the media as they can be assimilated to similar ellipsoids that present slightly same orientations. We will present in this part cells orientations measurement, and a way to quantify solid and porous anisotropy by calculating tortuosity on each phase.

The 3D inertia matrix is determined for each segmented cell. The 3 principal axes of the ellipsoid are denoted respectively by a, b and c with c< b<a. The referential O,x,y,z, is determined by the initial physical sample orientation during X-ray tomography process. The plane Oxy is the image plane, whereas the z direction is the thickness of the sample. Directions associated with each axis (a, b, and c) are determined using the eigenvectors associated to eigenvalues of the cell 3D inertia matrix. Figure 5 presents the elevation of the a,b and c axis into the 0-180° quadrant. The orientation distributions are quite narrow. The smallest cell axes (b and c) are almost horizontal, located into the plane O,x,y, and the a axis which correspond to the direction of the highest dimension of the cells are rather vertical (deviation is approximately 20°). The weak difference between b and c mean orientation values shows up that the plane O,b,c is not completely parallel to the sample image plane (O,x,y) as b- and c- axes are, by construction, orthogonal to a-axis.

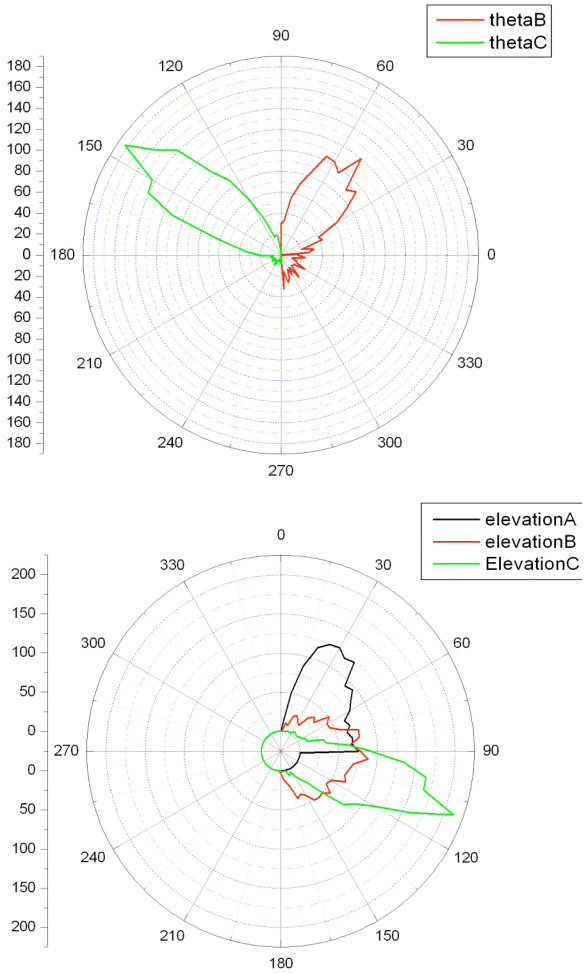

Figure 5. Azimuth and elevation distribution of the axes of the equivalent ellipsoid (3743 sample)

Tortuosity of a porous medium was for the first time defined by [10], in a particular direction, like the square of the ratio of the average effective distance traversed by the

fluid at the Euclidean distance between 2 sections.
We propose to measure a geometrical tortuosity based on geodesics calculation. We calculate the shortest path with the dijkstra's algorithm on the networks describing each phase. To highlight structural anisotropy we also measure tortuosity on box shape for different rotations around the Z axis.

To measure the tortuosity in a given direction (e.g. X-direction), we fix the source vertices at the plane (x0, y, z) and the arrival vertices at the plane (x1, y, z). First we define the tortuosity between a plane and a vertex:

$$\tau(x0,v) = \frac{1}{|x_v - x_0|} \min_{i \in S}\left(d_i[v]\right),$$

$$with\ d_i[v] = d[v]\ starting\ from\ s_i$$

S ={si, vertices of the starting surface}, V ={vj, vertices of the arrival surface } and N is the cardinal of the set V.

The tortuosity between the two planes is then simply defined as the arithmetic mean on all the arrival nodes:

$$\tau = \frac{1}{N} \sum_{j \in V} \tau(x0, v_j)$$

Figure 6 and 7 presents angular tortuosity variation for different box shaped skeleton respectively for the porous and the solid phase.

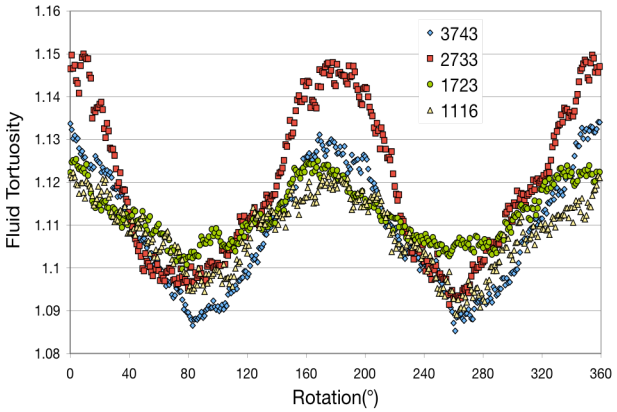

Figure 6.Fluid phase tortuosity

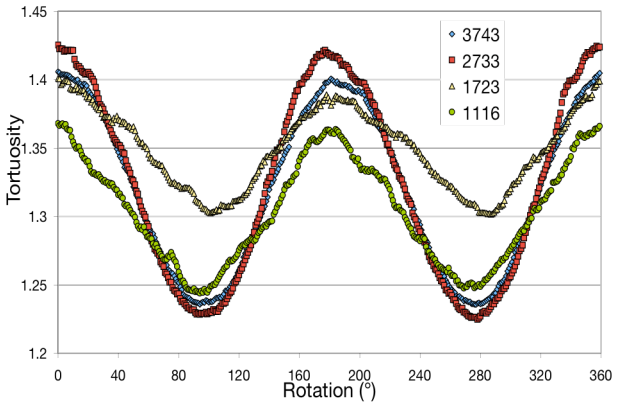

Figure 7.Solid skeleton tortuosity

Tortuosities are sinusoidal with a period of 180°. These results show clearly that tortuosities depend on direction and that the foam structure is slightly anisotropic. Solid and porous tortuosity are in phase and correlated to cells orientation [8].

CONCLUSION

We developed a morphological analysis tool to quantify the main structural parameters of metallic foams. It provides the functions of geometrical measurements. Cell shapes are measured and specific cell orientations are quantified. An original method based on graph theory has been developed to measure the geometrical tortuosity of both phases. Anisotropy of the solid matrix and fluid phase are observed. All analyzed foams present homothetic characteristics.

REFERENCES

1. Bastawros, A.F., A.G. Evans, and H.A. Stone, *Evaluation of cellular metal heat transfer media*. 1998, Harvard University Report.
2. Vicente, J., et al. *Structural properties measurement :A Morphological tool for transport properties determination* in *4th Int. Conf. on "Porous Metals and Metal Foaming Technology*. 2005. Kyoto, Japan.
3. Zeghondy, B., E. Iacona, and J. Taine, *Determination of the anisotropic radiative properties of a porous material by Radiative Distribution Function Identification (RDFI)*. Int. J. Heat and Mass Transfer, 2006.
4. Meyer, F.B., S., *Morphological segmentation*. Journal of Visual Communication and Image Representation, 1990. **1**: p. 21–46.
5. Dillard, T., et al. *In-situ observation of tensile deformation of open-cell nickel foams by means of X-ray microtomography* in *3rd International Conference on Cellular Metals and Metal Foaming Technology (MetFoam 2003*. 2003. (Germany).
6. Beucher, S. *Numerical residues*. in *7th International Symposum on Mathematical Morphology*. 2005. Paris.
7. Brun Emmanuel, et al., *Characterization of the full thermal conductivity tensor of anisotropic metal foams – Influence of fluid the phase.*, in *Metfoam 2007*. 2007: Montreal, Canada.
8. Vicente, J., et al. *Thermal conductivity of metallic foam: simulation on real x-ray tomographied porous medium and photothermal experiments* in *IHTC13, 13TH International Heat Transfer Conference*. 2006. Sydney.
9. Sethian, J.A., *Level Set Methods and Fast Marching Methods*. 1999, Cambridge, UK, : Cambridge University Press.
10. Carman, P.C., *Fluid flow through granular bed*. Trans. Instn Chem. Engrs., 1937. **15**: p. 150-156.